Numerical Properties of Constraint-Preserving Boundary Conditions for a Second Order Wave Equation

Alexander M. Alekseenko*

Department of Mathematics, California State University Northridge, Northridge, CA, 91330-8313, USA

Abstract. We implement Rung-Kutta discontinuous Galerking methods for the solution of second order vector wave equation and compare the performance of three sets of differential boundary conditions in the case when the solution is subject to the divergence-free constraint. Each set of boundary conditions produced a stable evolution with the numerical solution converging consistently with the method's order. One set of boundary conditions, the constraint preserving set, has been found to produce no reflected wave in the divergence of the discrete solution. A technique for constraint-damping was implemented in the equations. However the damping technique does not improve violations of the constraint originating at the boundary.

AMS subject classifications: 35L05,65M60

Key words: discontinuous Galerkin methods, wave equation, constraint-preserving boundary conditions.

1 Introduction

Problems in which governing evolution equations are coupled to differential constraint equations are common in mathematics. Important examples of such problems include electromagnetism, incompressible fluid dynamics and general relativity. Equations of relativity have the property of preserving the constraint equations in the following sense: symmetric hyperbolic equations satisfied by the unknowns imply symmetric hyperbolic evolution of the constraint quantities. As a result, if the initial data satisfies the constraint equations, the evolution equations will guarantee that the solution satisfies the constraint equations automatically at least in the domain of dependence on the initial data. However, perturbations of the constraint equations may enter the solution through the domain boundaries unless boundary conditions that are consistent with the constraint equations are used. Such boundary conditions, called the constraint-preserving

*Corresponding author. *Email address:* alexander.alekseenko@csun.edu (A.M. Alekseenko)

boundary conditions (CPBCs), have been introduced for the solution of Einstein's equations (cf. [8, 10, 17] and references therein). Because CPBCs are usually not in any standard form, the energy-based well-posedness proofs usually cannot be applied to them. Instead, the generalized well-posedness [16, 18] of the resulting systems is studied. The generalized well-posedness, however, often leaves questions on whether the CPBCs are suitable for discretizations by the standard techniques. This is why we consider a numerical implementation of the CPBCs developed in [3] for the wave equation subject to the divergence-free constraint. Our discretization is done by Runge-Kutta discontinuous Galerkin (RKDG) methods (cf. [1, 11, 12]). To formulate Runge-Kutta temporal discretization, the equations are reduced to the first order in time form. We compare the performance of three sets of boundary conditions. The first set controls incoming radiation condition for each component of the solution. The second set also controls incoming radiation, however the components are the incoming characteristic variables of the weak formulation. The third condition enforces the zero incoming radiation condition in the evolution of the constraint quantity [3] and is not in any standard form. Each set produces a stable evolution with the numerical solution converging with the expected order. The difference between the three boundary conditions, however, becomes apparent when one considers the constraint quantity. Namely, the third set of conditions does not produce spurious reflected waves in the divergence of the discrete solution while producing reflections in other components of the solution when the approximate zero incoming radiation conditions are specified. Moreover, the spurious reflections in the constraint quantity corresponding to the first two boundary conditions do not converge with resolution. We therefore conclude that the use of CPBCs can essentially improve simulations of systems with differential constraints.

Equations of electrodynamics were employed previously as a test bed for techniques in numerical general relativity (cf. [3, 9, 20, 23]). In [20] an extension of the Maxwell equations, the so-called fat Maxwell system, was studied. The solution was obtained for different sets of boundary conditions including constraint-preserving conditions. Our results are in agreement with this work, however there are important differences in our approaches. The first an possibly the most important difference is that we use a different set of constraint-preserving boundary conditions. The second difference is that our equations are solved in second order in space form as compared to the first order form that most of the simulations in numerical relativity use. We demonstrate that DG methods may be applied to the discretization of second order in space formulations of relativity. Examples of such formulations include the generalized harmonic and the BSSN formulations. Application of DG methods to simulation of scalar wave equation in second order form was considered in [14]. The theoretical framework for the stability of the scalar solution was established in [1]. In [1] it is discussed that the DG method for the second order semi-discretized equation is strongly unstable unless jump of the scalar solution across the element face is penalized. The present paper extends some of these results to the vectorial case. It was verified experimentally that only the jumps in components whose normal derivatives appear in the flux need to be penalized. The stable values of

the penalty factor are, however, larger that those of the scalar case.

The paper is organized as follows. A brief summary of notations and the problem formulation are given in Sections 2 and 3. Section 4 is dedicated to the description of the damping technique. In Section 5 we outline the numerical method. Finally, Section 6 is dedicated to the numerical results.

2 Notations

Our main unknown is $u_i(x,t):\Omega\times[0,T]\to\mathbf{R}^3$, where the set $\Omega\subset\mathbf{R}^3$ is a polyhedron. Lowercase Roman indices, e.g., i, j, k, etc., take values from 1 to 3. The vector n_i is the outward pointing unit normal to $\partial\Omega$. Also, u_n represents for the components of u_i normal to the boundary and ∂_n the derivative in the direction of n_i. We use capital Roman letters to denote vectors components tangential to the boundary, e.g., u_A and ∂_A. These tangential components can be evaluated by applying a projection operator $P^i_A=\delta^i_A-n_An^i$. Here δ^i_j is the unit matrix. We use tensorial notations in which repeated indices denote summation. Indices are raised and lowered by the unit matrix. For an array w_{ij}, $w_{(ij)}=(w_{ij}+w_{ji})/2$ is the symmetric and $w_{[ij]}=(w_{ij}-w_{ji})/2$ is the anti-symmetric part.

3 Formulation of the problem

In a cylinder $(x,t)\in\Omega\times[0,T]$ we consider the problem of solving the wave equation

$$\partial_t^2u_i=\partial^l\partial_lu_i, \tag{3.1}$$

coupled to a differential constraint

$$\partial^lu_l=0. \tag{3.2}$$

Formulations of initial-boundary value problems (IBVPs) for evolution systems with differential constraints has been recently extensively studied in applications to general relativity (cf. [8, 10, 23, 24]). Methods for deriving well-posed formulations and consistent boundary conditions were proposed in (cf. [3,10,19,25]). In [3] well-posed boundary conditions for (3.1) and (3.2) were constructed using a reduction of (3.1) to the form which evolves the constraint quantity statically. Theoretical well-posedness of the new boundary conditions were studied in the same work. In the present paper the new boundary conditions are tested numerically. Equation (3.1) is solved by Runge-Kutta discontinuous Galerkin (RKDG) methods using different sets of boundary conditions. We reduce (3.1) to first order in time and second order in space form. In this form, the system resembles the BSSN formulation of general relativity (cf. [2,7]). This way we will test the applicability of RKDG methods to the solution of such systems.

A direct numerical implementation of (3.1) and (3.2) is complicated because the system is formally overdetermined. Indeed, (3.1) and (3.2) taken together represent four

equations for the three components of $u_i(x,t)$. By applying ∂^i to both sides of (3.1) we find that the constraint quantity, $C := \partial^l u_l$, satisfies a subordinate equation

$$\partial_t^2 C = \partial^l \partial_l C. \tag{3.3}$$

If the initial data $u_i(x,0)$ and $\partial_t u_i(x,0)$ are such that $C(0) = \partial_t C(0) = 0$, then (3.3) implies that the constraint equation (3.2) is satisfied automatically in the domain of dependence on the initial data. This property is often referenced as the constraint preservation property. This property suggests that a solution to (3.1), (3.2) may be obtained using the so-called free evolution approach which consists of solving (3.1) alone, while not enforcing but monitoring (3.2). It follows from (3.3), however, that constraint violating perturbations of the solution may enter through the domain boundaries unless boundary conditions that are consistent with (3.2) are introduced. Boundary conditions that guarantee $C = 0$ are called constraint-preserving.

We introduce a new variable $\pi_i = \partial_t u_i$ and reduce (3.1) to the first order form in time. Also, we replace the Laplace operator with the identity $\partial^l \partial_l u_i = 2\partial^l \partial_{[l} u_{i]} + \partial_i \partial^l u_l$ to obtain

$$\begin{aligned} \partial_t u_i &= \pi_i, \\ \partial_t \pi_i &= 2\partial^l \partial_{[l} u_{i]} + \partial_i \partial^l u_l. \end{aligned} \tag{3.4}$$

Recall that n_i be the unit normal to $\partial\Omega$ pointing outward, and u_n and u_A denote the normal and tangential components of u_i, respectively. Also, $\partial_n = \partial^i n_i$ and ∂_A denote the normal and tangential derivatives on $\partial\Omega$, respectively. We will now introduce the three sets of boundary conditions we shall study. The first set consists of radiation-controlling conditions specified for each component of u_i:

$$\partial_t u_i + \partial_n u_i = \alpha(\partial_t u_i - \partial_n u_i) + h_i. \tag{3.5}$$

These boundary conditions are the most natural choice when the $\Delta = \operatorname{div}\nabla$ weak representation of the Laplace operator is used. Since most of the results found in the literature use this representation, in this paper we will reference (3.5) as the **standard** boundary conditions.

The second condition controls the incoming characteristic variables in the first order representation of (3.4) (see (4.1)):

$$\begin{aligned} \partial_t u_A + \partial_n u_A - \partial_A u_n &= \alpha(\partial_t u_A - \partial_n u_A + \partial_A u_n) + f_A, \\ \partial_t u_n + \partial^l u_l &= \beta(\partial_t u_n - \partial^l u_l) + f. \end{aligned} \tag{3.6}$$

In the case of $\alpha = \beta = 0$, $f_A = 0$ and $f = 0$ these conditions give the natural boundary conditions to the weak formulation of (3.4) in the sense of [4]. We therefore will refer to (3.6) as the **natural** boundary conditions.

The third condition was introduced in [3]:

$$\begin{aligned} \partial_t u_A + \partial_n u_A - \partial_A u_n &= \alpha(\partial_t u_A - \partial_n u_A + \partial_A u_n) + g_A, \\ \partial_t u_n + \partial_n u_n &= -\alpha(\partial_t u_n - \partial_n u_n) + g. \end{aligned} \tag{3.7}$$

If $\partial_t g = -\partial^A g_A$, then from (3.7) we have

$$\partial_t C + \partial_n C \quad = \quad \alpha(\partial_t C - \partial_n C) \quad \text{on} \quad \partial\Omega.$$

In view of (3.3), boundary conditions (3.7) imply that C remains zero if it is zero initially. Therefore (3.7) will be referenced as the **constraint-preserving** boundary conditions.

4 Constraint damping

An elegant and yet powerful technique for controlling the growth of constraints consists of adding special terms to the evolution equations. The added terms must not radically alter the nature of the equations, i.e., they must be low order and proportional to perturbations of constraint. Additionally, the added terms must force small perturbations of constraints to decay exponentially in time (cf. [6, 9, 15, 20]).

In order to construct damping terms, we introduce new variables $\varphi_{li} = 2\partial_{[l} u_{i]}$ and $\psi = \partial^l u_l$ and reduce the system to first order form:

$$\begin{aligned}
\partial_t u_i &= \pi_i; \\
\partial_t \pi_i &= 2\partial^l \varphi_{li} + \partial_i \psi; \\
\partial_t \varphi_{li} &= \partial_{[l} \pi_{i]}; \\
\partial_t \psi &= \partial^l \pi_l.
\end{aligned} \tag{4.1}$$

We are interested in solutions that satisfy $\psi = 0$. Therefore, we replace (4.1) with

$$\begin{aligned}
\partial_t u_i &= \pi_i, \\
\partial_t \pi_i &= 2\partial^l \varphi_{li} + \partial_i \psi, \\
\partial_t \varphi_{li} &= \partial_{[l} \pi_{i]}, \\
\partial_t \psi &= \partial^l \pi_l - \lambda \psi.
\end{aligned} \tag{4.2}$$

where $\lambda > 0$. Notice that any solution to (4.2) that satisfies $\psi = 0$ also solves (4.1) and vice versa. The boundary conditions for (4.2) are inferred from (3.7) by replacing derivatives of u_i with their expressions using the new variables. Setting $\alpha = 0$, $g_A = 0$ and $g = 0$ for simplicity, we obtain

$$\begin{aligned}
\pi_A + 2\varphi_{nA} &= 0, \\
\pi_n + \partial_n u_n &= 0.
\end{aligned} \tag{4.3}$$

A short calculation (cf. [3]) shows that values of ψ at the boundary must satisfy

$$\partial_t \psi + \partial_n \psi = -\lambda \psi. \tag{4.4}$$

Let a solution to (4.2) be found such that ψ is independent of time. By solving the last equation for $\partial^l \pi_l$ and using it in the left side of the second equation, we find that ψ is a

harmonic function. Then $\psi=0$ due to (4.4). Furthermore, one can show that $\partial^l u_l=\partial_t\partial^l u_l=0$. We notice also that by solving the last equation in (4.2) for ψ and substituting the result into the second equation we obtain a system that only involves π_i and φ_{li}. The decoupled equations can be reduced to the first order symmetric hyperbolic form. Therefore both π_i and φ_{li} may be recovered from the initial and boundary data.

Now let us consider a solution in which ψ depends on time. By differentiating the third equation of (4.2) in time and substituting the second equation for $\partial_t\pi_i$ we obtain

$$\partial_t^2\psi=\partial^l\partial_l\psi-\lambda\partial_t\psi.$$

A standard calculation verifies that any solution of (4.2) and (4.3) satisfies the energy identity

$$\frac{1}{2}\partial_t(\|\partial_t\psi\|^2+\|\partial_l\psi\|^2+\lambda\|\psi\|^2_{\partial\Omega})=-\int_{\partial\Omega}(\partial_t\psi)^2-\lambda\|\partial_t\psi\|^2, \tag{4.5}$$

where $\|\cdot\|^2$ stands for the suitable L_2-norm on Ω, e.g., $\|\psi\|^2=\int_\Omega\psi^2$ and $\|\varphi_i\|^2=\int_\Omega\varphi_i\varphi^i$. Also, $\|\psi\|^2_{\partial\Omega}=\int_{\partial\Omega}\psi^2 d\sigma$. It follows from (4.5) that $\mathcal{E}(t):=\|\partial_t\psi\|^2(t)+\|\partial_l\psi\|^2(t)+\lambda\|\psi\|^2_{\partial\Omega}(t)$ is non-increasing. More specifically, $\mathcal{E}(t)\le\mathcal{E}(0)$ and $\mathcal{E}(0)$ grows with λ at most linearly.

We drop the first term in the right side of (4.4) and move the second to the left side. Multiplying the result by a factor of $e^{2\lambda t}$ after regrouping we obtain

$$\partial_t(\|\partial_t\psi\|^2e^{2\lambda t})+e^{2\lambda t}\partial_t(\|\partial_l\psi\|^2+\lambda\|\psi\|^2_{\partial\Omega})\le 0.$$

Integration with respect to time yields

$$\|\partial_t\psi\|^2e^{2\lambda t}+\int_0^t e^{2\lambda\tau}\partial_\tau(\|\partial_l\psi\|^2+\lambda\|\psi\|^2_{\partial\Omega})d\tau\le\|\partial_t\psi\|^2(0).$$

We now integrate by parts in the second term to obtain

$$\|\partial_t\psi\|^2+\|\partial_l\psi\|^2+\lambda\|\psi\|^2_{\partial\Omega}\le\mathcal{E}(0)e^{-2\lambda t}+\int_0^t e^{2\lambda(\tau-t)}(\|\partial_l\psi\|^2+\lambda\|\psi\|^2_{\partial\Omega})d\tau. \tag{4.6}$$

The second term in the right side can be made small by choosing λ large enough. Also, the first term is exponentially decreasing in time. (In fact, we expect that the second integral is also exponentially decreasing in time.) Therefore solutions of (4.2) are expected to approach $\psi=$constant. Finally, the third term in (4.6) guarantees that this constant must be zero. In practice, however, we need to take into the account the truncation errors that will perturb the numerical solution on every time step. These perturbations can be perceived as the random initial data for ψ. We therefore expect that rather than converging to zero, $\|\psi\|$ will approach the level of truncation errors and will remain at that level. The larger the value of the parameter λ is the faster $\|\psi\|$ will reach the steady state.

By solving the last equation of (4.2) for ψ and integrating the third in time, we rewrite the constraint-damped equations in second order in space form:

$$\partial_t u_i=\pi_i;$$
$$\partial_t\pi_i=2\partial^l\partial_{[l}u_{i]}+\partial_i\partial^l u_l-\lambda\int_0^t e^{2\lambda(\tau-t)}\partial_i\partial^l u_l d\tau.$$

This form of the equations, however, is not convenient for the numerical implementation. Instead, we introduce $\Phi_i = \int_0^t e^{2\lambda(\tau-t)}\partial_i\partial^l u_l$ as a new variable and re-write the system as [21,22]

$$\begin{aligned}
&\partial_t u_i = \pi_i,\\
&\partial_t \pi_i = 2\partial^l \partial_{[l} u_{i]} + \partial_i \partial^l u_l - \lambda\Phi_i,\\
&\partial_t \Phi_i = \partial_i \partial^l u_l - \lambda\Phi_i.
\end{aligned} \tag{4.7}$$

The numerical solution of (4.7) is discussed in the next two sections.

5 The numerical method

We will now outline the discontinuous Galerkin formulation used to solve (4.7). Let the polyhedral domain Ω be partitioned into elements K_α. (In the examples discussed in the next section rectangular domains and partitions are used.) Only the discretization of the second equation will be considered; the derivation is similar for the third equation. We assume that on each K_α the approximate solution belongs to the space of polynomials of degree at most k, $P^k(K_\alpha)$. Contracting the equation with a test function $v^i(x)$ and integrating over K_α, we obtain after integration by parts:

$$\begin{aligned}
\int_{K_\alpha} \partial_t \pi_i v^i = &-\int_{K_\alpha} [2(\partial_{[l} u_{i]})(\partial^{[l} v^{i]}) + (\partial^l u_l)(\partial_i v^i)] - \int_{K_\alpha} \lambda\Phi_i v^i\\
&+ \int_{\partial K_\alpha} [(\partial_n u_A - \partial_A u_n) v^A + (\partial^l u_l) v^n], \qquad \forall v^i \in P^k(K_\alpha).
\end{aligned} \tag{5.1}$$

Here n_i is the outward pointing normal vector to ∂K_α and v^n stands for the normal and v^A for the tangential components of v^i on ∂K_α.

To define a discontinuous Galerkin (DG) method one needs to replace the boundary integral with a numerical flux. To this end, we rewrite the integrand as

$$\begin{aligned}
\frac{1}{2}\Big\{ &(\partial_t u_A + \partial_n u_A - \partial_A u_n) v^A - (\partial_t u_A - \partial_n u_A + \partial_A u_n) v^A\\
&+ (\partial_t u_n + \partial^l u_l) v^n - (\partial_t u_n - \partial^l u_l) v^n \Big\}
\end{aligned}$$

and notice that $\partial_t u_A + \partial_n u_A - \partial_A u_n$ and $\partial_t u_n + \partial^l u_l$ are the incoming and $\partial_t u_A - \partial_n u_A + \partial_A u_n$ and $\partial_t u_n - \partial^l u_l$ are the outgoing characteristic variables of the weak formulation. We will employ the upwind numerical flux which consists of replacing the incoming fields with their limiting values from the outside of K_α and the outgoing fields with their limiting values from the inside. As is discussed in [1,4] DG discretizations are strongly unstable unless terms penalizing the solution jump across the element face are included in their formulations. By introducing penalty terms for each component of u_i whose normal

derivatives appear in the numerical flux, we arrive at the DG discretization of (5.1). The penalty terms are precisely taken to be

$$\int_{\partial K_\alpha} \frac{D(s)}{d(K_\alpha)} [[u_i]] \nu^i. \tag{5.2}$$

Here $[[u_i]] = \lim_{\varepsilon \to 0^+} u_i(t, x_j + \varepsilon n_j) - \lim_{\varepsilon \to 0^-} u_i(t, x_j + \varepsilon n_j)$ denotes the jump across the face ∂K_α. The parameter $d(K_\alpha)$ is related to the linear dimensions of the element. For rectangular elements, it is defined to be equal to the distance from ∂K_α to the opposite face. It is not clear, however, what choice of $d(K_\alpha)$ works best for more general meshes. The parameter $D(s)$ is a penalty parameter, it increases with the order of the method. In [1] values of $D(s)$ that guarantee stable DG discretizations of second order scalar wave equation are proposed. Our simulations suggest that the stable values of $D(s)$ for (5.1) are slightly larger that those of [1]. However, our system is vectorial and thus essentially different from the scalar case.

The treatment of the flux on the outside boundary $\partial\Omega$ requires a special mention. Three sets of boundary conditions were implemented: (3.5), (3.6) and (3.7). We recall that (3.6) is closely related to the natural conditions of the weak formulation (5.1) in the sense of [4]. Therefore, we will reference to (3.6) as the natural boundary conditions. At the same time, neither (3.5) nor (3.7) can be conveniently expressed in terms of the characteristic variables of the weak formulation (5.1). A different weak formulation can be proposed for (3.1) such that (3.5) is a combination of the characteristic variables. This formulation, in fact, corresponds to the perhaps most familiar representation of the Laplace operator, $\Delta = \operatorname{div} \nabla$. Because of the familiarity, we will reference to (3.5) as the standard boundary conditions. Finally, boundary conditions (3.7) will be referred to as the constraint-preserving conditions. It does not seem possible to propose a weak formulation of (3.1) for which (3.7) can be described in terms of the incoming and outgoing characteristic variables. Thus it is unlikely that (3.7) can be formulated as an upwind flux condition for (3.1). However (3.7) implies a well-posed dissipating flux condition for (3.3). To implement the boundary conditions we assume the continuity of u_i at the boundary and substitute expressions (3.6), (3.5) and (3.7) for the corresponding portions of the flux. To illustrate this on an example, consider the first equation of (3.7). The corresponding terms in the flux are

$$(\partial_t u_A + \partial_n u_A - \partial_A u_n)\nu^A - (\partial_t u_A - \partial_n u_A + \partial_A u_n)\nu^A.$$

We rewrite these as

$$(\partial_t u_A + \partial_n u_A - \partial_A u_n)\nu^A - \alpha(\partial_t u_A - \partial_n u_A + \partial_A u_n)\nu^A - (1-\alpha)(\partial_t u_A - \partial_n u_A + \partial_A u_n)\nu^A$$

and use (3.7) to replace the first two terms, obtaining the expressions for the boundary flux implemented in the numerical method

$$g_A - (1-\alpha)(\partial_t u_A - \partial_n u_A + \partial_A u_n)\nu^A.$$

Now we consider the second equation of (3.7). Terms in the flux that correspond to this equation are

$$(\partial_t u_n + \partial^l u_l)v^n - (\partial_t u_n - \partial^l u_l)v^n.$$

We rewrite these as

$$(\partial_t u_n + \partial_n u_n) + \alpha(\partial_t u_n - \partial_n u_n) - ((1+\alpha)\partial_t u_n - (1+\alpha)\partial_n u_n - 2\partial^A u_A)$$

and substitute (3.7) for the first two terms to obtain the implemented expressions. Finally, the jump penalty does not appear in the flux on the outside boundary because we assume that the function is continuous at the boundary from the inside and all expressions are evaluated in the interior of the element.

The rest of the derivation follows by introducing the basis functions in $P^k(K_\alpha)$ and following the standard procedure (cf. [11, 12]) to obtain a system of equations for the coefficients of the basis representation of the solution. The final expressions are rather cumbersome, therefore we omit them for the sake of space. Numerical simulations presented in the next section were obtained using the basis functions which are products of Legendre's polynomials on rectangular partitions. We used explicit Runge-Kutta schemes for integration in time. Schemes of orders up to five have been employed in simulations.

6 The numerical results

Boundary conditions (3.5)–(3.7) were employed in the simulation of the propagation of two-dimensional divergence-free waves. An exact divergence-free solution to (3.1) is given by

$$(\partial_{x_2} f(t - d_i x^i), -\partial_{x_1} f(t - d_i x^i)). \tag{6.1}$$

Our first experiment was concerned with the reconstruction of the solution corresponding to the profile function $f(\xi) = \sin(6\pi\xi)$ traveling in the direction $d_i = (1/\sqrt{2}, 1/\sqrt{2})$. The domain for simulations was a unit square, $[0,1]\times[0,1]$. The initial and boundary data were evaluated from the exact solution. In each simulation, the equations were solved for 10 crossing times using one of the boundary conditions (3.5)–(3.7). By the time $t = \sqrt{2}$ the exact solution is determined by the boundary data everywhere in the domain. We can therefore use (6.1) to test the ability of the boundary conditions (3.5)–(3.7) to approximate divergence-free solutions.

Results of the simulations of the periodic solution are presented in Figs. 1–3. In Fig. 1(a) the x-component of the exact solution is shown. In Figs. 1(b) and (c) the L_2-norms of the error and the local divergence are shown for solutions corresponding to different values of the jump penalty factor. The spatial discretization in these experiments was by polynomials of degree two on sixteen cells in both directions. The temporal discretization is by the optimal Runge-Kutta method of third order. Each consecutive line was obtained by doubling the penalty factor. As is seen in Fig. 1(b) the numerical solution is unstable

unless the jump penalty parameter is sufficiently large (cf. [1]). We observe that the error decreases as the penalty parameter increases which suggests that the optimal order of convergence in the DG method can be restored by a sufficiently large jump penalty. However, any further increase in the penalty factor requires a reduction of the time step at least by a factor of two. The fact that the time step must be reduced is a serious disadvantage of the implemented method. The situation, however, could have been improved by using implicit integration in time. Finally, in Fig. 1(c) the divergence of the solution is shown for different values of the jump penalty factor. It appears that for the half-value of the penalty parameter the solutions has already converged to a level when errors in divergence are dominated by truncation errors rather than spurious oscillations related to the discontinuity of the numerical solution.

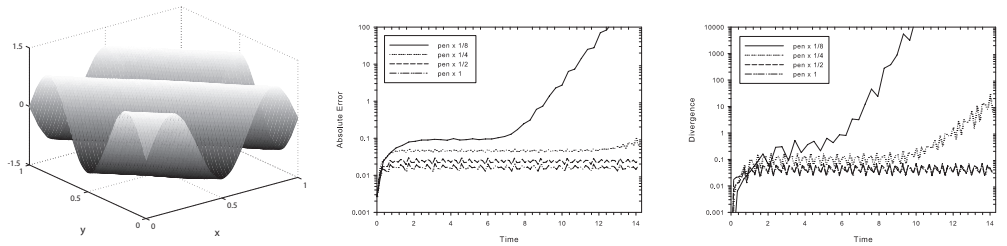

(a) (b) (c)

Figure 1: (a) the periodic plane wave; (b) the L_2-norm of the error and (c) the L_2-norm of the local divergence in solutions corresponding to different values of the jump penalty.

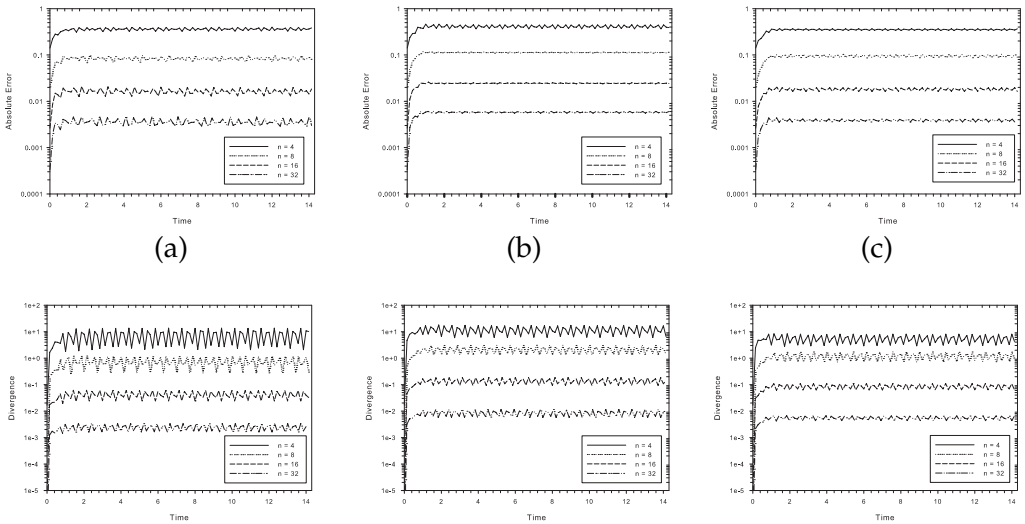

(a) (b) (c)

(d) (e) (f)

Figure 2: The error and the local divergence in simulations of a periodic plane wave.

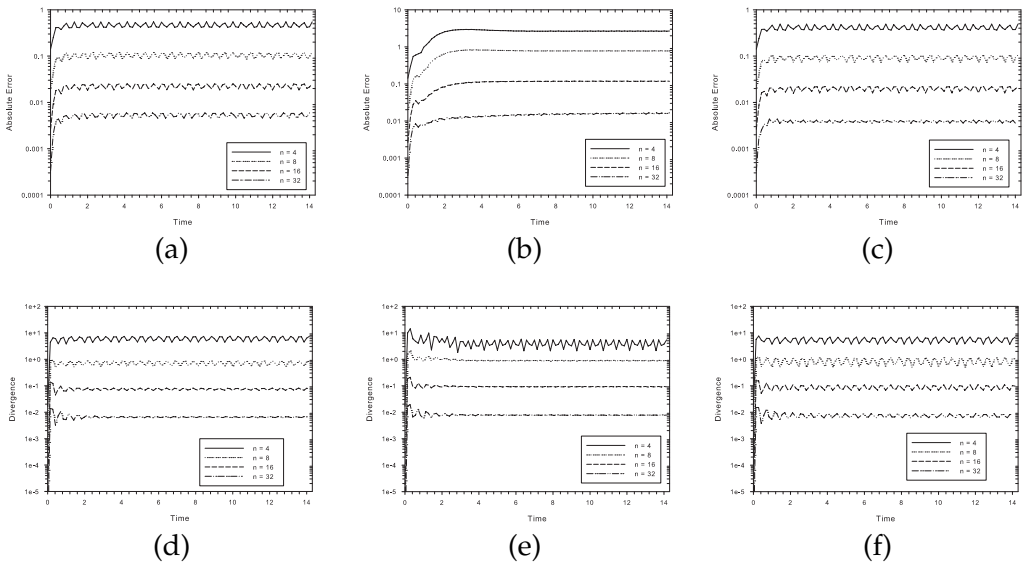

Figure 3: The error and the local divergence in simulations of a periodic plane wave. Constraint damping was employed with $\lambda = 32$.

Solutions corresponding to different boundary conditions are compared in Figs. 2 and 3. Simulations without constraint damping are shown in Fig. 2. The L_2-norm of the error is plotted in Figs. 2 (a), (b) and (c) and the local divergence in Figs. 2(d), (e) and (f). Figs. 2(a) and (d) correspond to boundary conditions (3.6), Figs. 2(b) and (e) to (3.5) and Figs. 2(c) and (f) to (3.7). We notice that the error is slightly less in the case of (3.6) as compared to (3.5) and (3.7). Notice that the L_2-norm of the error appears to converge with the second order only. This may be improved by using larger values of the jump penalty but will result in significantly slower calculations. The local divergence, in contrast, converges with order better than three. Again, the divergence is about half a digit smaller in the case of (3.6) than that of (3.5) and (3.7). However, it oscillates more. Overall, in this experiment conditions (3.6) perform better than the constraint-preserving boundary conditions (3.7). This suggests that if the boundary data is known exactly, the best results are obtained by using boundary conditions that are natural for the weak formulation. However the difference between the solutions was not great.

In Fig. 3 the solutions using constraint damping are presented. The value of the damping parameter in these experiments is $\lambda = 32$, all other parameters are as in the previous experiment. Here, again, Figs. 3(a) and (d) correspond to boundary conditions (3.6), Figs. 3(b) and (e) to (3.5) and Figs. 3(c) and (f) to (3.7). The absolute error in the numerical solution is shown in Figs. 3(a), (b) and (c). We notice that the error increased in the case of (3.6), however, the error oscillations became smaller. The errors for other boundary conditions did not change significantly. The value of the divergence has slightly increased in all three simulations. This may appear surprising since the damping term was designed

to suppress the divergence exponentially in time. However, according to the estimate (4.6), rather then driving the divergence to zero, the damping term forces it to return to the levels determined by the initial data. Because the truncation errors in the solution generate initial data for the divergence on every time step, the damping term is expected to drive the local divergence to the level prescribed by the truncation errors. We thus conclude that unless the equation has the property of magnifying small perturbations of the constraints, for example due to nonlinear terms, the use of constraint damping is not justified in view of its computational costs.

Our second experiment is concerned with the propagation of a divergence-free flat pulse. The exact solution has the form of (6.1) where the profile function was taken to be

$$f(\xi)=a\exp\Big(\frac{b}{(\xi-r_1)(\xi-r_2)}\Big).$$

The pulse is moving toward the X-axis at an angle of incidence of $\pi/6$. Matching boundary data was evaluated using the exact solution.

Results of the simulations are presented in Figs. 4 and 5. In Fig. 4(a) the x-component of the exact solution is shown. In Figs. 4(b) and (c) the convergence of the absolute error and the divergence are shown in the case of the constraint-preserving boundary conditions. As in the previous experiment, the order of convergence is below the optimal and is slightly better than second for the second degree polynomial DG approximation. It is observed that the absolute error increases as the pulse hits the corner of the domain and dissipates exponentially after the pulse leaves the domain. The local divergence in the numerical solution behaves similarly: it is the greatest when the pulse hits the corner and exponentially decreases when the pulse leaves. It appears as plausible, therefore, that in this problem perturbations of the constraint are largely determined by the errors originating at the domain boundary. This observation will be further evidenced by the propagation of a circular divergence-free pulse.

In Fig. 5 solutions corresponding to different boundary conditions are compared. The discretizations in the interior of the domain and in time are the same in all experiments. Solutions obtained without constraint damping, with $\lambda=0$, are shown in Fig. 5(a) and (c) and solutions obtained using the constraint damping technique, with $\lambda=32$, are shown in Fig. 5(b) and (d). In the case of propagation without constraint damping, performance of all three conditions is about the same with the constraint-preserving boundary conditions performing a notch better. In the case of constraint damping, the boundary conditions (3.6) tend to give fastest damping of the divergence and have the smallest error once the pulse leaves the domain. Notice that during the time when the pulse is still passing through the boundary, the use of damping does not result in any improvement in the divergence. Overall, the perturbations of the constraint originating at the boundary make the largest contribution to the total constraint violation. Moreover, such perturbations are not treatable by the damping technique of the Section 4.

Our third experiment is concerned with the propagation of a divergence-free circular pulse. The pulse is given by the solution to the wave equation corresponding to the initial

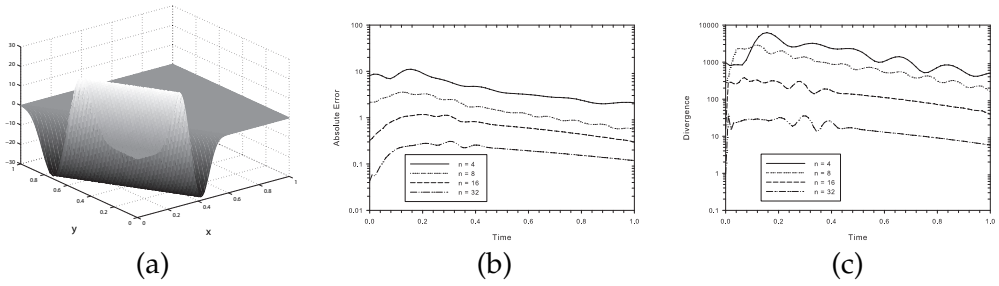

(a) (b) (c)

Figure 4: Propagation of a flat divergence-free pulse by a third order RKDG method. (a) the exact solution; (b) and (c) convergence of the error in (b) and the divergence in (c) in the numerical solution using the constraint-preserving boundary conditions.

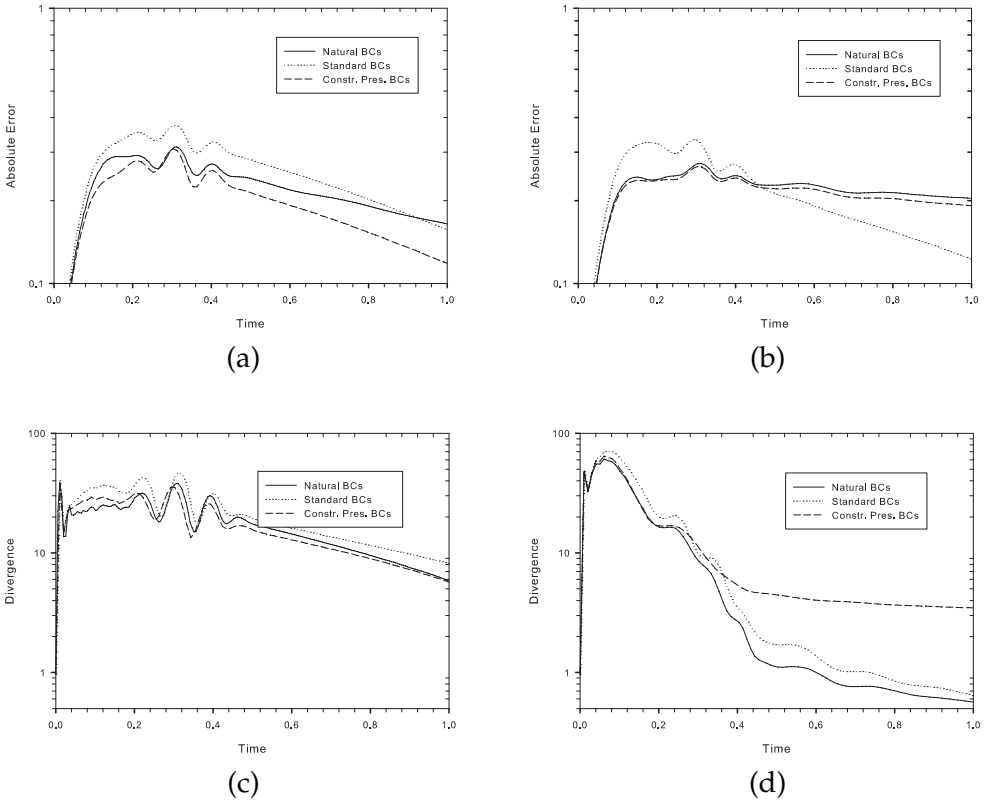

(a) (b) (c) (d)

Figure 5: Propagation of a flat divergence-free pulse for different boundary conditions: (a) and (c) correspond to simulations with no constraint damping and (b) and (d) to simulations with constraint damping with $\lambda = 32$.

data

$$u_i(0,x) = (\partial_{x_2} h(0,x), -\partial_{x_1} h(0,x)) \quad \text{and} \quad \partial_t u_i(0,x) = (\partial_{x_2}\partial_t h(0,x), -\partial_{x_1}\partial_t h(0,x)),$$

where

$$h(t,x) = a\exp\Big(\frac{b}{r^2(t,x) - r_*^2}\Big), \quad r(t,x) = -s(t-t_0) + \sqrt{(x-x_0)^2 + (y-y_0)^2}.$$

By the construction, the initial data is divergence-free. Moreover, the support for the pulse is located strictly inside the domain. Therefore perturbations of the constraint that are due to the truncation errors inside the domain will appear first. The perturbations that originate at the boundary will appear only after the pulse has reached the boundary. Because the exact solution is not known in closed form, the homogeneous radiation-controlling conditions are imposed at the boundary. Specifically, we set $\alpha = \beta = 0$, $h = 0$, $f_A = g_A = 0$, $f = g = 0$ in (3.5)–(3.7). We compare the L_2-norm and the local divergence of the solutions for each of the three boundary conditions.

The results of simulations by a third order RKDG method are shown in Figs. 6 and 7. In Fig. 6(a) the x component of the circular pulse is shown. In Figs. 6(b) and (c) the divergence is plotted for solutions using (3.7) and (3.6) respectively. During the time when the pulse has not yet reached the boundary, the divergence in the solutions converges with better than the third order in both simulations. However, when the pulse reaches the boundary at the time $t = .2$, differences can be observed. The constraint-preserving boundary conditions (3.7) allow the solution to leave without perturbing the constraint significantly. Spurious reflections are however generated in the numerical solution with errors having the same L_2-norm as for the other boundary conditions (see Fig. 7). In contrast, the natural boundary conditions generate spurious reflections that largely perturb the constraint (see Fig. 6(c)). Moreover, the constraint perturbations do not converge with resolution once the pulse hits the boundary. This suggests that the constraint is very sensitive to the replacement of the matched boundary data by the approximate condition of no incoming radiation. In Fig. 7 the solutions L_2-norm and the local divergence are compared for each of the three boundary conditions. Simulations without constraint damping are shown in Figs. 7(a) and (c) and simulations with constraint damping corresponding to the value of the parameter $\lambda = 32$ are shown in Figs. 7(b) and (d). Notice that after the time $t = .4$ the exact solution is expected to leave the domain entirely. Therefore, after the time $t = .04$ the numerical solutions consist of the spurious reflections only. We notice that for all simulations, the L_2-norm of the solutions is about the same, however the difference is observed in the L_2-norm of the divergence. The smallest reflection in the divergence is observed for the constraint-preserving boundary conditions (3.7) while the natural conditions (3.6) perform the worst at this time. The divergence decreases faster in simulations with constraint damping. A decrease in divergence is also noticeable in Fig. 7(d) shortly before the pulse reaches the boundary. We therefore conclude that the damping technique (4.7) can reduce violations of the constraint that are due to the truncation errors inside the domain. However, as was discussed previously, damping is not effective in controlling violations of the constraint that are introduced at the boundary.

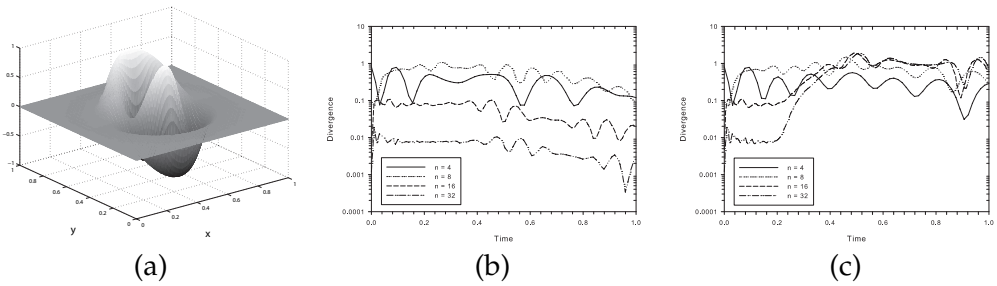

Figure 6: Propagation of a circular divergence-free pulse by a third order RKDG method. (a) the exact solution; (b) and (c) convergence of the divergence in the numerical solution using constraint-preserving boundary conditions in (b) and natural boundary conditions in (c).

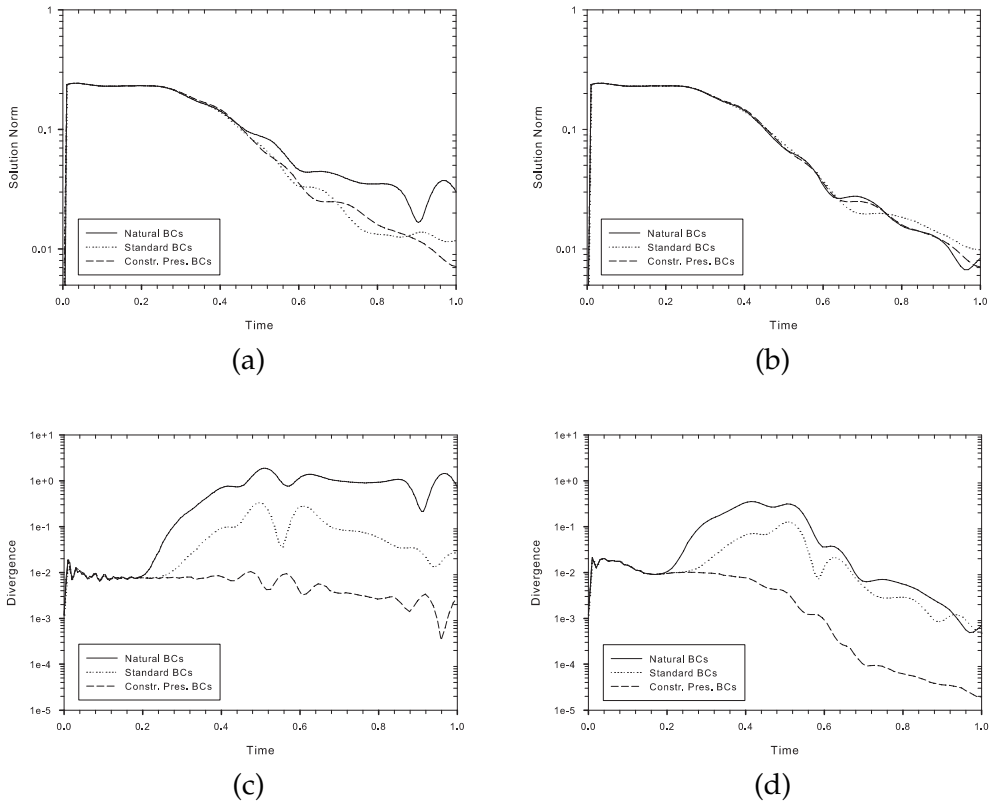

Figure 7: Propagation of a circular divergence-free pulse for different boundary conditions: (a) and (c) correspond to simulations with no constraint damping and (b) and (d) to simulations with constraint damping with $\lambda = 32$.

7 Conclusions

We performed simulations of vector wave equation in second order form using high order RKDG methods. The performance of three sets of boundary conditions was studied. We found that the constraint-preserving boundary conditions did not produce reflections in the solution's divergence while the approximate zero incoming radiation conditions produced reflections that did not converge with resolution. A constraint damping technique similar to that of [6, 15, 20] was implemented. When zero incoming radiation conditions are imposed at the boundary, the damping forces the L_2 norm of the constraint to decrease exponentially. However, even in this case, damping did not decrease the divergence during the times when the pulse was passing the artificial boundary. When matching boundary data was computed from the known exact solution, the damping technique did not improve simulations either. We therefore conclude that unless the equation has a property to magnify small perturbations of the constraints, e.g., due to nonlinear terms, the use of constraint damping is not justified in view of their computational costs. In agreement to [20] constraint violations did not converge when the approximate zero incoming radiation conditions were used. This fact may have important consequences since approaches has been proposed in relativity to employ high order transparent boundary conditions to reduce reflections in the constraint quantity (cf. [8]). Therefore, it will be interesting to perform numerical simulations using high order analogs of the zero incoming radiation conditions (cf. [5,13]) and investigate whether the constraint-violating reflections converge for high order transparent boundary conditions.

8 Acknowledgement

The author acknowledges the support of CSUN Research, Scholarship and Creative Activity Awards program. The author thanks Peter Monk, Lee Lindblom, Mark Scheel and Dan Givoli for numerous insightful discussions and suggestions. The author also thanks his friend Lorraine L. Foster for help in preparing the final version of this manuscript.

References

[1] M. Ainsworth, P. Monk, and W. Muniz. Dispersive and dissipative properties of discontinuous Galerkin finite element methods for the second-order wave equation. *J. Sci. Comput.*, 27(1–3), 2006.

[2] M. Alcubierre, B. Brügmann, P. Diener, M. Koppitz, D. Pollney, E. Seidel, and R. Takahashi. Gauge conditions for long-term numerical black hole evolutions without excision. *Phys. Rev. D*, 67:084023, 2003. (`http://arXiv.org/abs/gr-qc/020672`).

[3] A. M. Alekseenko. Well-posed initial-boundary value problem for a constrained evolution system and radiation-controlling constraint-preserving boundary conditions. *J. Hyperbolic Differ. Equ.*, 4(4):1–26, 2007. (`http://arXiv.org/abs/gr-qc/0611011`).

[4] D. N. Arnold, F. Brezzi, B. Cockburn, and L. D. Marini. Unified analysis of discontinuous Galerkin methods for elliptic problems. *SIAM J. Numer. Anal.*, 39(5):1749–1779, 2001/02.

[5] Alvin Bayliss and Eli Turkel. Radiation boundary conditions for wave-like equations. *Communications on Pure and Applied Mathematics*, 33(6):707–725, 1980.

[6] Othmar Brodbeck, Simonetta Frittelli, Peter Hubner, and Oscar A. Reula. Einstein's equations with asymptotically stable constraint propagation. *Journal of Mathematical Physics*, 40(2):909–923, 1999.

[7] B. Brügmann, W. Tichy, and N. Jansen. Numerical simulation of orbiting black holes. *Phys. Rev. Lett.*, 92:211101, 2004. (`http://arXiv.org/abs/gr-qc/0312112`).

[8] Luisa T Buchman and Olivier C A Sarbach. Towards absorbing outer boundaries in general relativity. *Classical and Quantum Gravity*, 23(23):6709–6744, 2006.

[9] G. Calabrese. A remedy for constraint growth in numerical relativty. *Class. Quant. Grav.*, 21:4025–4040, 2004.

[10] G. Calabrese, J. Pullin, O. Sarbach, M. Tiglio, and O. Reula. Well-posed constraint-preserving boundary conditions for the linearized Einstein equations. *Commun. Math. Phys.*, 240:377–395, 2003. (`http://arXiv.org/abs/gr-qc/0209017`).

[11] B. Cockburn. Discontinuous Galerkin methods for convection-dominated problems. In T. Barth and H. Deconink, editors, *High-order methods for computational physics*, volume 9 of *Lect. Notes Comput. Sci. Eng.*, pages 69–224. Springer-Verlag, Berlin, 1999.

[12] B. Cockburn. Discontinuous Galerkin methods. *ZAMM Z. Angew. Math. Mech.*, 83(11):731–754, 2003.

[13] Dan Givoli. High-order nonreflecting boundary conditions without high-order derivatives. *J. Comput. Phys.*, 170(2):849–870, 2001.

[14] Marcus J. Grote, Anna Schneebeli, and Dominik Schotzau. Discontinuous galerkin finite element method for the wave equation. *SIAM Journal on Numerical Analysis*, 44(6):2408–2431, 2006.

[15] Carsten Gundlach, Gioel Calabrese, Ian Hinder, and Jose M Martin-Garcia. Constraint damping in the z4 formulation and harmonic gauge. *Classical and Quantum Gravity*, 22(17):3767–3773, 2005.

[16] B. Gustafsson, H.-O. Kreiss, and J. Oliger. *Time Dependent Problems and Difference Methods*. Wiley & Sons, New York, 1995.

[17] L. E. Kidder, L. Lindblom, M. A. Scheel, L. T. Buchman, and H. P. Pfeiffer. Boundary conditions for the Einstein evolution system. *Phys. Rev. D*, 71:064020, 2005. (`http://arXiv.org/abs/gr-qc/0412116`).

[18] H.-O. Kreiss and J. Lorenz. *Initial-Boundary Value Problems and the Navier-Stokes Equations*. Academic Press, San Diego, 1989.

[19] H.-O. Kreiss and J. Winicour. Problems which are well-posed in a generalized sense with applications to the Einstein equations. *Class. Quant. Grav.*, 23:S405–S420, 2006. (`http://arXiv.org/abs/gr-qc/0602051`).

[20] L. Lindblom, M. A. Scheel, L. E. Kidder, H. P. Pfeiffer, D. Shoemaker, and S. A. Teukolsky. Controlling the growth of constraints in hyperbolic evolution systems. *Phys. Rev. D*, 69:124025, Jun 2004.

[21] Lee Lindblom, Keith D. Matthews, Oliver Rinne, and Mark A. Scheel. Gauge drivers for the generalized harmonic einstein equations. *Physical Review D*, 77:084001, 2008.

[22] Lee Lindblom and Bela Szilagyi. Improved gauge driver for the generalized harmonic einstein system. *Physical Review D (Particles, Fields, Gravitation, and Cosmology)*, 80(8):084019, 2009.

[23] O. Reula and O. Sarbach. A model problem for the initial-boundary value problem of Einstein equations. *J. Hyperbolic Differ. Equ.*, 2(2):397–435, 2005.

[24] O. Rinne. Stable radiation-controlling boundary conditions for the generalized harmonic Einstein equations. *Class. Quant. Grav.*, 23(22):6275–6300, 2006. (`http://arXiv.org/abs/gr-qc/0606053`).

[25] Olivier Sarbach and Manuel Tiglio. Boundary conditions for einstein's field equations: Analytical and numerical analysis. *Journal of Hyperbolic Differential Equations*, 2:839, 2005.